2016

Low Temperature Solution-Processed Sb:SnO_2 Nanocrystals for Efficient Planar Perovskite Solar Cells

Yang Bai
University of Nebraska-Lincoln, ybai@unl.edu

Yanjun Fang
University of Nebraska-Lincoln, jkfang@zju.edu.cn

Yehao Deng
University of Nebraska-Lincoln

Qi Wang
University of Nebraska-Lincoln, qwang15@unl.edu

Jingjing Zhao
University of Nebraska-Lincoln, jzhao27@unl.edu

See next page for additional authors

Published in *ChemSusChem* 9 (2016), pp 2686–2691. doi 10.1002/cssc.201600944

Submitted July 15, 2016; revised August 17, 2016; published online August 26, 2016.

Low Temperature Solution-Processed Sb:SnO_2 Nanocrystals for Efficient Planar Perovskite Solar Cells

Yang Bai, Yanjun Fang, Yehao Deng, Qi Wang, Jingjing Zhao, Xiaopeng Zheng, Yang Zhang, and Jinsong Huang

Department of Mechanical and Materials Engineering, Nebraska Center for Materials and Nanoscience University of Nebraska-Lincoln Lincoln (USA)

Corresponding author — J. Huang, email jhuang2@unl.edu

Abstract
Inorganic metal oxide electron-transport layers (ETLs) have the potential to yield perovskite solar cells with improved stability, but generally need high temperature to form conductive and defect-less forms, which is not compatible with the fabrication of flexible and tandem solar cells. Here, we demonstrate a facile strategy for developing efficient inorganic ETLs by doping SnO_2 nanocrystals (NCs) with a small amount of Sb using a low-temperature solution-processed method. The electrical conductivity was remarkably enhanced by Sb-doping, which increased the carrier concentration in Sb:SnO_2 NCs. Moreover, the upward shift of the Fermi level owing to doping results in improved energy level alignment, which led to reduced charge recombination, and thus longer electron recombination lifetime and improved open-circuit voltage (V_{OC}). Therefore, Sb-doping of SnO_2 significantly enhanced the photovoltaic performance of planar perovskite devices by increasing the fill factor and V_{OC}, and reducing photocurrent hysteresis, extending the potential application of low-temperature-processed ETLs in future flexible and tandem solar cells.

Keywords: doping, low temperature, perovskite solar cells, stability, tin oxide

Introduction

Organometal trihalide perovskite solar cells are emerging as a promising new generation of photovoltaic technology owing to the unprecedented rise in their power conversion efficiency (PCE) from 3.8%[1] to 22.1%[2] in the span of a few years. So far the record top-performing perovskite solar cells usually employ mesoporous TiO_2 (m-TiO_2) as the electron transport layer (ETL), which also plays a key role in reducing the photocurrent hysteresis.[3] However, the desired high temperature (>400 8°C) for processing m-TiO_2 increases the fabrication cost and prevents the use of lightweight and flexible substrates. In addition, perovskite solar cells based on m-TiO_2 degrade faster under UV illumination,[4] which is a critical challenge for practical application in terms of long term stability. Therefore, wide-bandgap semiconductor metal oxides, such as ZnO, In_2O_3, SnO_2, and Zn_2SnO_4, have been investigated as potential alternatives to TiO_2.[5] Among them, SnO_2 has attracted tremendous attention as a promising and effective ETL material for high performance perovskite solar cells because of its nature-abundant element, low cost, excellent chemical stability, and high electron mobility (100–200 cm^2V^{-1} s^{-1}), suggesting faster transport of photo-injected electrons to the transparent conductive oxide current collector. Moreover, in comparison with TiO_2 and ZnO, SnO_2 has a wider band gap (3.6–3.8 eV), which would create fewer oxidative holes in the valence band, resulting in significantly improved photostability under UV illumination. The lower conduction band minimum (CBM) of SnO_2 would promote the charge injection. Fang et al. reported solution-processed SnO_2 ETLs for planar perovskite solar cells with PCE over 17%.[5e] Nonetheless the SnO_2 films were thermally annealed at a high temperature over 180 °C for 1 h, which is still too high to be well compatible with the roll-to-roll manufacturing of perovskite devices and detrimental to most plastic flexible substrates with working temperature below 155°C.[6] Later on, Hagfeldt et al. increased the efficiency of planar perovskite solar cells employing SnO_2 as the ETL to achieve a PCE of 18.4% by atomic layer deposition (ALD) of high quality SnO_2 films.[5d] In terms of energy band alignment with mixed perovskite $(FAPbI_3)_{0.85}(MAPbBr_3)_{0.15}$, SnO_2 is more favorable in comparison with TiO_2 and showed less energy mismatch owing to the deeper conduction band,[5d] in addition to its less absorption in near UV range. Despite of the high PCE achieved, ALD is not a scalable, low-cost deposition method for large-scale manufacturing. More recently, SnO_2 nanoparticles (NPs) were synthesized by either sol-gel or hydrothermal methods as ETL materials for perovskite solar cells.[5f, 7] However, the performance of perovskite devices incorporating solely SnO_2 nanoparticles as ETLs were far from satisfied and the photocurrent hysteresis in these devices was severe, which can be explained by the large density of surface traps of the assynthesized

SnO_2 NPs with low conductivity. These SnO_2 films still need to be covered by a thin layer of TiO_2 or fullerene to reduce trap densities at the SnO_2 surface and to suppress charge recombination at the interface between SnO_2 and perovskite.[5f, 7]

Here, we report the successful synthesis of highly crystalline Sb-doped SnO_2 (Sb:SnO_2) nanocrystals (NCs) through a facile low-temperature solution-process method, and their application as ETL materials for efficient n-i-p planar perovskite solar cells. The thermal annealing temperature for spin-coated Sb:SnO_2 films is reduced to as low as 100 °C. The introduction of Sb increases the electron concentration, and thus enhances the film conductivity over one order of magnitude and reduces solar cell photocurrent hysteresis in comparison with the pristine SnO_2. The extra free electrons partially fill the surface trap states and shift the Fermi level upward, leading to reduced charge recombination and thus improved PCE of perovskite devices from 15.7 to 17.7% (steady state efficiency).

Results and Discussion

In a typical synthesis of SnO_2 nanocrystals (NCs), acetic acid and tetramethylammonium hydroxide were used to adjust the pH of the precursor solution to nearly neutral values, which was identified to be beneficial for the crystallization of SnO_2 NPs.[8] In addition to the reaction pH, the ratio of water and viscous ethylene glycol allows for the sophisticatedly controlled hydrolysis of metal species, leading to well-dispersed SnO_2 NCs without precipitation for several months. The intentional incorporation of atomic substitutions into semiconductor materials for doping or alloying has been demonstrated as an effective approach for tailoring optoelectronic properties, such as band gap or conductivity.[9] Previous studies showed that the best conductivity was achieved in SnO_2 doped with 3–5 mol% Sb, which was the result of an optimum combination of high charge-carrier concentration and high mobility.[9d] However, the Sb content cannot be too high, because it would otherwise raise the effective activation energy of the donor and rapidly decrease the carrier mobility owing to increased disorder or scattering. In this work, a small amount of Sb (2, 4, and 10 mol%) was introduced as the n-dopant for SnO_2 NCs. The preliminary results of performance testing shown in Figure S1 (in the Supporting Information) indicate that 4 mol% is the optimum doping content, which was used in the following in-depth study. The incorporation of a small amount of Sb^{5+} as n-dopant would induce a shallow donor level formed close to the conduction band of SnO_2.[9d, 10] Synthesis of the pristine SnO_2 resulted in the formation of white particles dispersion, while the color of the resultant colloidal dispersion changed to brownish when the Sb source was added to the reaction system.

The crystallographic structures of the as-synthesized pristine SnO_2 and Sb: SnO_2 NCs were examined by X-ray diffraction (XRD) measurements as shown in Figure 1a. It was observed that all diffraction peaks, including (110), (101), (211), and (112), can be well indexed to tetragonal rutile SnO_2 (JCPDS card: 41-1445) for pristine and doped NCs. No additional diffraction peaks from other secondary crystalline impurities were detected. This indicates that the antimony dopants are evenly distributed and do not cause obvious disruption of the SnO_2 lattice structure. A

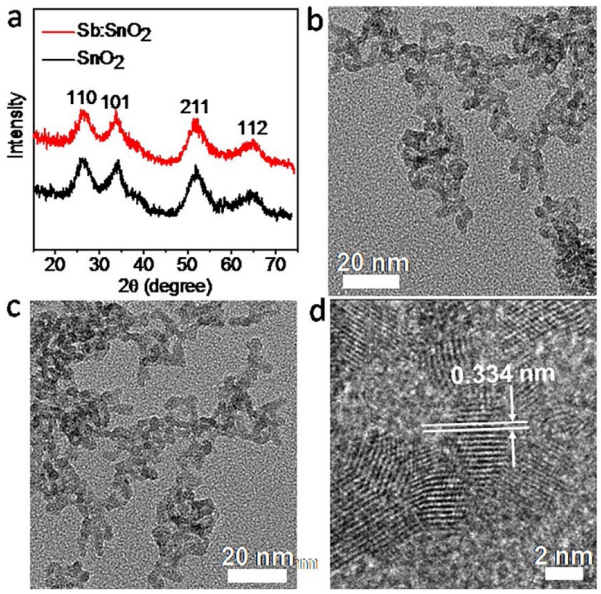

Figure 1. (a) XRD patterns of as-synthesized SnO_2 and Sb:SnO_2. (b–c) TEM images of SnO_2 and Sb:SnO2 NCs, respectively. (d) HRTEM image of Sb:SnO_2 NCs.

previous study showed that the SnO_2 lattice can accommodate up to 30 mol% Sb atoms without significant structure changes.[9d] Yet the intensity of the diffraction peaks slightly reduced and the full-width at half maximum (FWHM) increased a little bit in the case of Sb:SnO_2, which is consistent with a previous report that the incorporation of Sb into the SnO_2 crystal lattice caused a decrease in the crystalline domain size.[9c, 11] Transmission electron microscopy (TEM) was used to characterize the morphology of the pristine and doped NCs as shown in Figure 1b and c, respectively. The NCs are extremely small and have diameters in the range of 2– 4 nm. Figure 1d exhibits the representative high resolution TEM (HRTEM) image of Sb:SnO_2 NCs. The clear lattice fringes observed in the HRTEM image further confirm the high crystallinity of these NCs. The outer d spacing is measured to be approximately 0.334 nm, corresponding to the interplanar spacing of (110) plane of rutile SnO_2.

The SnO_2 and Sb:SnO_2 films were deposited on indium tin oxide (ITO) substrates by spin-coating their colloidal NC dispersion. The top-view scanning electron microscopy (SEM) images shown in Figure 2a and b revealed that the films were smooth and pinhole free. The NCs are too small to distinguish individual particles on the film by SEM, and the extremely small size is highly favorable in producing continuous and smooth ETL films. As displayed in Figure 2c, the ITO substrates coated with SnO_2 and Sb:SnO_2 films with similar thickness showed comparable transmittance spectra, which indicates the band gap has not been changed by doping with a low concentration of Sb. The improved light transmission compared to bare ITO substrates is consistent with a previous study,[5e] and of benefit to enhance the photocurrent and thus PCE for perovskite solar cells. To study the Sb doping effect, conductivity measurements of both pristine SnO_2 and Sb:SnO_2 films were performed with co-planar films coated on normal glass. The obtained current–voltage

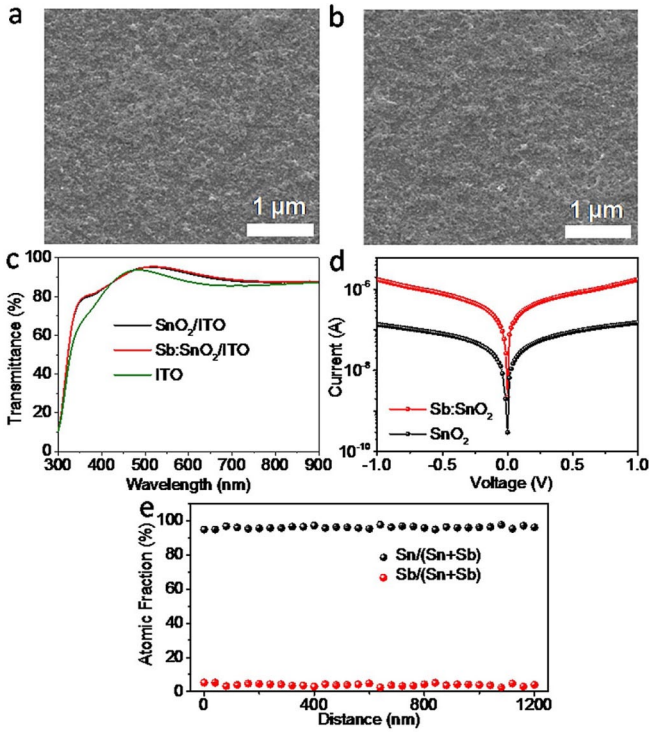

Figure 2. (a–b) Top-view SEM images of SnO2 and Sb:SnO_2 NC films deposited on ITO, respectively. (c) Transmission spectra of ITO substrates without and with a compact SnO_2 or Sb:SnO_2 NC film. (d) Comparison of the *I–V* characteristics of SnO_2 and Sb:SnO_2 NC films deposited on glass substrates. (e) EDX element line scan profile acquired across the Sb:SnO_2 film.

(*I–V*) curves are presented in Figure 2d. Clearly, the conductivity of Sb-SnO_2 dramatically increased over one order of magnitude in comparison with pristine SnO_2. This is most likely a result of increased carrier concentration. In addition, the extra electrons in the doped Sb:SnO_2 are expected to partially fill the charge traps in SnO_2. To investigate and further confirm the Sb-doping, bulk compositional analysis for the Sb:SnO_2 film was performed with energy-dispersive X-ray spectroscopy (EDX). Figure 2e shows the EDX element line scan profile acquired across the film indicating that the Sb-doping is homogeneously distributed within the film. The atomic fraction of Sb is calculated to be approximately 4%, which verified the amount of Sb incorporated into SnO_2 NCs.

To study the doping effect in depth and verify the significantly improved electrical conductivity, we constructed n-i-p planar perovskite solar cells that have a structure of ITO/SnO_2 or Sb:SnO_2 ETL/perovskite/hole transport layer (HTL)/Au electrode as illustrated in Figure 3a. The relevant energy levels such as the conduction band minimum (CBM) and valence band maximum (VBM) of each component layer in the device are presented in Figure 3b. The Fermi level of SnO_2 is closely related to the carrier concentration, and an increased electron concentration should push up the Fermi energy level of this n-type conductor. The amount of Fermi level shift can be estimated from the carrier concentration change with Equation (1), assuming the carrier mobility remains same after doping:

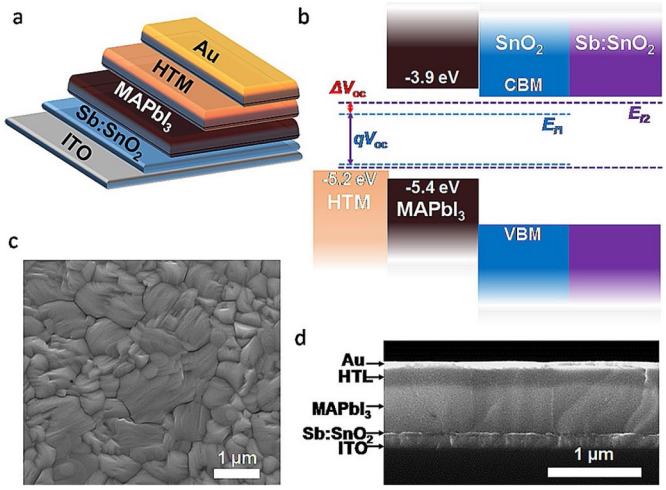

Figure 3. (a) Structure of the n-i-p planar perovskite solar cells. (b) Energy band diagram of the perovskite solar cells based on SnO_2 and Sb:SnO_2 ETLs. (c) Top-view SEM image of perovskite film coated on Sb:SnO_2. (d) Cross-sectional SEM image of a typical perovskite device based on Sb:SnO_2.

$$\frac{n_2}{n_1} = \exp\left(-\frac{E_{f2}-E_{f1}}{kT}\right) \quad (1)$$

where n_1 and n_2 are the carrier concentrations of the pristine and doped SnO_2, respectively, E_{f1} and E_{f2} are the Fermi levels of the pristine and doped SnO_2, respectively, k is the Boltzmann constant, and T is the temperature. The carrier concentrations were then obtained by performing Hall effect measurements on both films. After doping, the carrier concentration of the SnO_2 increased from 6.7×10^{21} to 8.2×10^{22} m^{-3}, thus the upward shift of Fermi level after doping is calculated to be around 60 meV. The lifted Fermi level of doped SnO_2 matches better with the electron quasi-Fermi level of $CH_3NH_3PbI_3$ under illumination without dragging down the quasi-Fermi level splitting in the device, similar to the effect of reduced energy disorder in fullerene ETL as we reported previously.[12] This is expected to enhance the open-circuit voltage (V_{OC}) of the solar cells, which was indeed observed in this study.

To fabricate the perovskite solar cells, the $CH_3NH_3PbI_3$ films were prepared using the two-step interdiffusion approach, where PbI_2 and methyl ammonium iodide were sequentially spun onto the SnO_2- and Sb:SnO_2-coated ITO substrates, followed by a solvent annealing process.[13] Figure 3c shows the typical compact perovskite films achieved on Sb:SnO_2 ETL with an average grain size larger than 1 mm. 2,2′,7,7′-Tetrakis-(*N*,*N*-di-4-methoxyphenylamino)-9,9′-spirobifluorene (Spiro-OMeTAD) co-doped with Li_+ and Co_+ as the hole-transport material (HTM) was then spin-coated on top of the perovskite films. The devices were completed by thermal evaporation of a top Au electrode. Detailed information on film and device fabrication can be found in the Experimental Section. The cross-section SEM image of a typical device is presented in Figure 3d.

The photocurrent density–voltage (*J–V*) characteristics of the perovskite solar cells based on SnO_2 and Sb:SnO_2 ETLs are

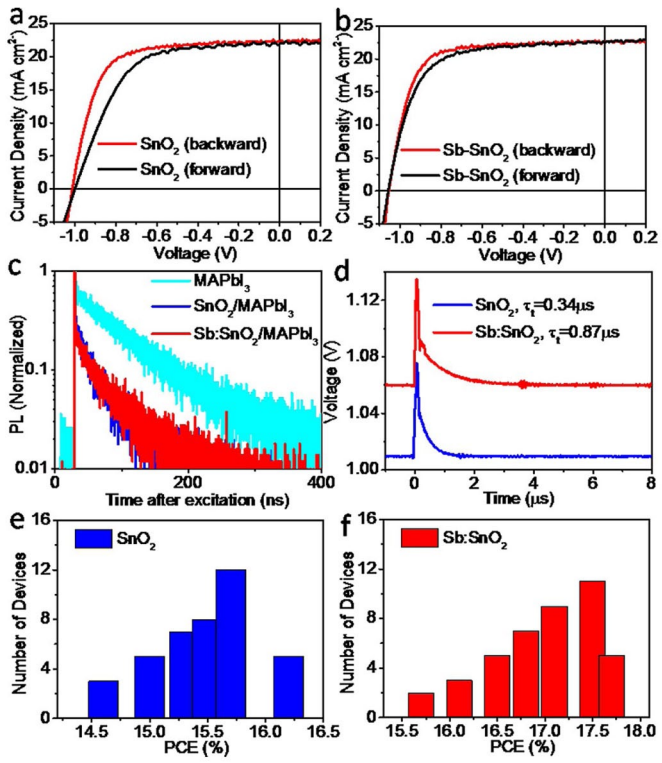

Figure 4. (a–b) *J–V* curves of perovskite devices based on SnO_2 and Sb:SnO_2 ETLs measured with different sweep directions (backward and forward). (c) Normalized time-resolved PL decay curves of the CH3NH3PbI3 layer on its own and CH3NH3PbI3 at the interfaces with SnO_2 and Sb:SnO_2 ETLs. (d) Normalized transient photovoltage decay curves based on SnO_2 and Sb:SnO_2 ETLs under one sun illumination. (e–f) Statistics of the PCE distribution for perovskite devices with SnO_2 (40 devices) and Sb:SnO2 (42 devices).

shown in Figure 4a and b, respectively, measured under AM1.5G irradiation (100 mWcm^{-2}) with different sweeping directions (backward and forward). It is noted that the perovskite solar cells using a compact layer of pristine SnO_2 as the ETL exhibited significant hysteresis. The typical perovskite device with SnO_2 measured under backward voltage scan direction had a V_{OC} of 1.01 V, a photocurrent density (J_{SC}) of 22.3 mAcm^{-2}, and a fill factor (FF) of 69.6 %, yielding a PCE of 15.7 %. When measured under a forward voltage scan, the same device showed comparable J_{SC} and V_{OC} but significantly reduced FF of 59.7 %, which resulted in a lower PCE of 13.2 %. Very encouragingly, the V_{OC} and FF increased dramatically to 1.06 V and 72.0 %, respectively, in the typical perovskite device employing Sb:SnO_2 ETL, resulting in an enhanced PCE of 17.2% under backward voltage scan. Moreover, the Sb:SnO_2 device exhibited much less hysteresis with a PCE of 16.2% measured under forward voltage scan. All the photovoltaic parameters of these perovskite devices are summarized in Table 1. Such a great enhancement in photovoltaic performance reveals the crucial role of Sb-doping. As discussed previously, the electrical conductivity was remarkably increased in Sb:SnO_2 ETLs and interfacial electron transport was facilitated, leading to enhanced FF. Furthermore, the improvement of V_{OC} was nearly equal to the upward shift of Fermi level calculated

Table 1. Photovoltaic performance of perovskite devices based on SnO_2 and Sb:SnO_2 measured with different sweep directions.

Sample	Sweep direction	J_{SC} [mAcm^{-2}]	V_{OC} [V]	FF [%]	PCE [%]
SnO_2	backward	22.3	1.01	69.6	15.7
	forward	22.1	1.00	59.7	13.2
Sb:SnO_2	backward	22.6	1.06	72.0	17.2
	forward	22.5	1.06	67.8	16.2

from the carrier concentration change upon Sb-doping. This indicates there is no shift of conduction band.

To gain further insight into the reasons for the performance enhancement induced by the Sb-doping, the charge-carrier transfer and photo-generated charge recombination lifetime were characterized by time-resolved photoluminescence (TRPL) decay and transient photovoltage (TPV) decay. Figure 4c shows the TRPL decay of the $CH_3NH_3PbI_3$ films on various substrates, including bare ITO and SnO_2- and Sb:SnO_2-coated ITO substrates. As can be seen, the $CH_3NH_3PbI_3$ film on ITO showed a much slower PL decay, indicating slow carrier recombination in the perovskite layer. When brought into contact with the n-type electron extraction layers, the PL decay were accelerated to a comparable rate for both pristine and Sb-doped SnO_2 contacts. Therefore, the Sb-doping has a negligible influence on the electron injection from $CH_3NH_3PbI_3$ to SnO_2. However, the charge recombination lifetime (0.87 ms) of the Sb:SnO_2 device, deduced from TPV decay curves measured under one sun illumination as illustrated in Figure 4d, was substantially longer than that (0.34 ms) of the device with pristine SnO_2. The longer charge recombination lifetime indicates the suppressed interfacial charge recombination, which was attributed to Sb-doping. As discussed above, increasing the carrier concentration by Sb-doping significantly improved the conductivity. We speculate it would slightly alleviate the charge accumulation at the interface of the perovskite with ETL. Additionally, the excessive donated electrons are supposed to partially fill the trap states, which also leads to reduced recombination and thus enhanced V_{OC}.[10, 14] The statistics of PCE distributions shown in Figure 4e and f not only demonstrate the promise of the Sb:SnO_2 ETL, but also the reliability and reproducibility of the PCE enhancement achieved by the Sb-doping effect.

Figure 5a specifically depicts the photovoltaic performance of the optimized device based on Sb:SnO_2 ETL with a J_{SC} of 22.5 mAcm^{-2}, a V_{OC} of 1.06 V, and a FF of 74.2 %, yielding a PCE of 17.7 %. The corresponding external quantum efficiency (EQE) spectrum is plotted in Figure 5b, for which the integrated J_{SC} agrees well with the value achieved in the *J–V* curve. To further confirm the device stability and reliability of the perovskite device, the steady-state photocurrent and efficiency measured at the maximum power point (–0.89 V) are presented in Figure 5c, where a stabilized PCE of 17.6% was obtained. There is still an increase in PCE with illumination, indicating the presence of some charge traps in the Sb:SnO_2 ETL. This agrees with the slight photocurrent hysteresis observed. In principle, it can be eliminated by blending Sb:SnO_2 with other passivating ETLs, such as [6,6]-phenyl-C_{61}-butyric acid methyl ester (PCBM), which is the focus of further study.

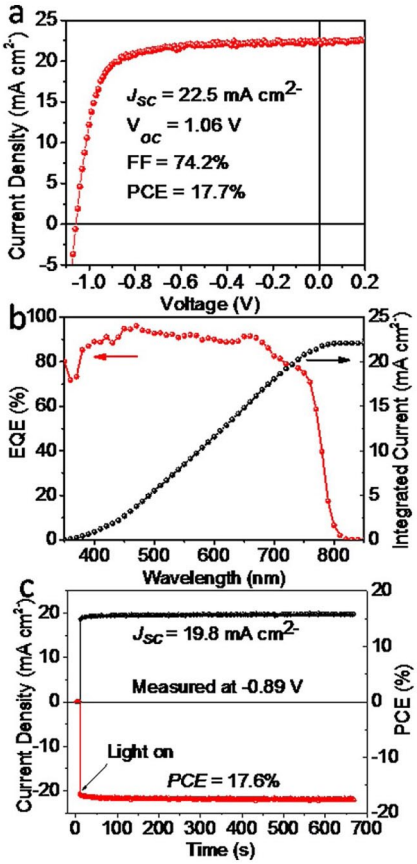

Figure 5. (a) *J–V* curve, (b) EQE, and (c) steady-state photocurrent and PCE at the maximum power point of the optimized perovskite solar cell based on Sb:SnO_2.

A preliminary study of long-term durability was also performed on devices that were stored in a desiccator out of the glovebox under room light. As shown in Figure S2, over 95% of the original PCE can be retained after storage for 21 days. On the other hand, the demonstration of a low-temperature solution-processed fullerene-free metal oxide ETL has a significant impact on future stable perovskite/silicon tandem device development. The concern on the instability of fullerene is removed by using pure oxide ETLs. It assures much longer operation lifetime owing to its robust nature against H_2O, O_2, and UV light. Moreover, it acts as a tri-functional layer when deposited on top of perovskite layer in silicon/perovskite tandem solar cells as part of the top transparent electrode, which extracts electrons, blocks the H_2O and O_2 from penetrating into the perovskite layer, and protects the underlying layers during the sputtering of the transparent conducting oxide electrode.

Conclusions

We report a facile low-temperature solution-processed nanocrystalline Sb:SnO_2 electron-transport layer (ETL) for efficient planar n-i-p perovskite solar cells with significantly reduced hysteresis and higher efficiency. Sb-doping was successfully demonstrated to dramatically enhance the electrical conductivity of SnO_2, which in turn enhanced the fill factor of the devices. Moreover, an upward shift in the Fermi level of the ETL induced by Sb-doping increased the device open-circuit voltage. This work represents an important step towards developing efficient and stable inorganic ETLs for high performance perovskite solar cells without resorting to organic passivation layers.

Experimental Section

Materials synthesis: SnO_2 NCs were prepared according to a modified method.[8b] $SnCl_4{\cdot}5H_2O$ (1 g) was added to a 100 mL flask and fully dissolved in 20 mL ethylene glycol by magnetic stirring for 30 min. Subsequently, acetic acid (2 mL) and of tetramethylammonium hydroxide (2–3 mL, 10% in water) were added dropwise to the flask immersed in an oil bath to well control the hydrolysis reaction. The resultant clear solution was first kept stirring at 100°C until it turned to a white cloudy mixture, which indicates the complete formation of SnO_2 nanoparticles. Ultimately, the solution was further refluxed at 170°C for 2 h. For the synthesis of Sb:SnO_2 NCs with different doping levels (2, 4, and 10 mol%), $SbCl_3$ was used as the dopant source. Upon completion of the reaction, the solution was centrifuged and the supernatant was discarded. The precipitates were re-dispersed in ethanol by ultrasonication. This washing process was repeated at least three times. The washed solids were finally dispersed again in ethanol at a concentration of 5–10 mgmL^{-1} for use to form compact films. Methylammonium iodide (CH_3NH_3I) was synthesized using the method described in our previous publication.[15]

Device fabrication: SnO_2 and Sb:SnO_2 films were first deposited on cleaned ITO substrates by spin coating the corresponding NC colloid solution at 2500 rpm for 30 s, followed by drying on a hot plate at 100°C. This procedure was repeated for three times to control the film thickness and the as-prepared films were further annealed at 100°C for 30 min in air. The $CH_3NH_3PbI_3$ films were prepared by our previously published solvent annealing-induced interdiffusion method.[13] PbI_2 [dissolved in *N*,*N*-dimethylformamide (DMF)] was spin-coated on top of SnO_2 or Sb:SnO_2/ITO substrates at 6000 rpm for 35 s. CH_3NH_3I (dissolved in 2-propanol) was spin-coated on top of the dried PbI_2 layer at room temperature at 6000 rpm for 35 s. Afterwards the stacked precursor layers were solvent-annealed at 100°C for 1 h. The HTL solution was spin-coated on top of the perovskite layer at 4000 rpm for 30 s, where spiro-OMeTAD in chlorobenzene (1 mL, 90 mgmL^{-1}) was employed with addition of lithium bis(trifluoromethanesulfonyl)imide (Li-TFSI) in acetonitrile (23 mL, 520 mgmL^{-1}), tris(2-(1H-pyrazol-1-yl)-4-*tert*butylpyridine) cobalt(III) tri[bis(trifluoromethane)sulfonimide in acetonitrile (50 mL, 100 mgmL^{-1}), and 4-*tert*-butylpyridine (27 mL). The devices were completed by thermal evaporation of Au (60 nm) as the top electrode. The device working area was 8 mm^2, as defined by the overlap of the ITO substrate and the Au cathode.

Film and device characterization: The XRD patterns of the NCs were obtained by a Bruker-AXS D8 Discover Diffractometer with CuKa radiation (wavelength of about 1.54 Å). TEM and HR-TEM analysis were carried out on a FEI OSIRIS microscope. The

transmission spectra of ITO substrates without and with SnO_2 or Sb:SnO_2 were obtained by using a LAMBDA 1050 UV-vis-NIR Spectrophotometer. The SEM images were taken from a Quanta 200 FEG environmental scanning electron microscope. The resistivity measurements of pristine SnO_2 and Sb:SnO_2 films that were deposited on glass were performed using a four-point probe setup as described in the previous work.[16] EDX line scan was carried out on a FEI Helios NanoLab™ 660 instrument equipped with TEAM energy dispersive spectroscope. The typical electron acceleration voltage for X-ray excitation was 10 kV. The typical acceleration current was 0.2 nA. The charge-carrier concentration of the pristine and doped films were studied by the Hall effect measurement, which was performed using a six-contacts Hall bar method.[17] The *J–V* curves of the devices were measured under AM1.5G irradiation (100 $mWcm^{-2}$), which was produced by a xenon-lamp-based solar simulator (Oriel 67005, 150W Solar Simulator). The light intensity was calibrated by a Schott visible-color glass-filtered (KG5 color-filtered) Si diode (Hamamatsu S1133) before photocurrent measurements. A Keithley 2400 Source-Meter was used for recording the *J–V* measurements. The bias scanning rate was 0.05 Vs^{-1}. The steady-state PCE was measured by recording the photocurrent at a bias voltage of –0.89 V. The EQE was obtained using a Newport QE measurement kit by focusing a monochromatic beam of light onto the devices. TRPL was measured by a Horiba DeltaPro time-correlated single photon counting system. The 404 nm pulsed laser diode was used as the excitation source with pulse width of 45 ps. The scattered laser was eliminated with a 650 nm long-pass filter. The detection wavelength range was selected by a 77 nm band-pass filter with band width of 10 nm. The TPV measurements were conducted under one sun illumination according to our previous work.[13]

Acknowledgments — The information, data, or work presented herein was funded by the Office of Energy Efficiency and Renewable Energy (EERE), U.S. Department of Energy, under Award Number DE-EE0006709.

References

[1] A. Kojima, K. Teshima, Y. Shirai, T. Miyasaka, *J. Am. Chem. Soc.* **2009**, *131*, 6050–6051.

[2] http://www.nrel.gov/ncpv/images/efficiency chart.jpg

[3] N. J. Jeon, J. H. Noh, Y. C. Kim, W. S. Yang, S. Ryu, S. I. Seok, *Nat. Mater.* **2014**, *13*, 897–903.

[4] T. Leijtens, G. E. Eperon, S. Pathak, A. Abate, M. M. Lee, H. J. Snaith, *Nat. Commun.* **2013**, *4*, 7410.

[5] a) D. Liu, T. L. Kelly, *Nat. Photonics* **2014**, *8*, 133–138;

b) Y. Dkhissi, S. Meyer, D. Chen, H. C. Weerasinghe, L. Spiccia, Y.-B. Cheng, R. A. Caruso, *ChemSusChem* **2016**, *9*, 687–695;

c) M. Qin, J. Ma, W. Ke, P. Qin, H. Lei, H. Tao, X. Zheng, L. Xiong, Q. Liu, Z. Chen, *ACS Appl. Mater. Interfaces* **2016**, *8*, 8460–8466;

d) J. P. Correa Baena, L. Steier, W. Tress, M. Saliba, S. Neutzner, T. Matsui, F. Giordano, T. J. Jacobsson, A. R. Srimath Kandada, S. M. Zakeeruddin, A. Petrozza, A. Abate, M. K. Nazeeruddin, M. Gratzel, A. Hagfeldt, *Energy Environ. Sci.* **2015**, *8*, 2928–2934;

e) W. Ke, G. Fang, Q. Liu, L. Xiong, P. Qin, H. Tao, J. Wang, H. Lei, B. Li, J. Wan, G. Yang, Y. Yan, *J. Am. Chem. Soc.* **2015**, *137*, 6730–6733;

f) H.-S. Rao, B.-X. Chen, W.-G. Li, Y.-F. Xu, H.-Y. Chen, D.-B. Kuang, C.-Y. Su, *Adv. Funct. Mater.* **2015**, *25*, 7200–7207;

g) L. S. Oh, D. H. Kim, J. A. Lee, S. S. Shin, J.-W. Lee, I. J. Park, M. J. Ko, N.-G. Park, S. G. Pyo, K. S. Hong, J. Y. Kim, *J. Phys. Chem. C* **2014**, *118*, 22991–22994;

h) S. S. Shin, W. S. Yang, J. H. Noh, J. H. Suk, N. J. Jeon, J. H. Park, J. S. Kim, W. M. Seong, S. I. Seok, *Nat. Commun.* **2015**, *6*, 4710;

i) J. Song, E. Zheng, J. Bian, X.-F. Wang, W. Tian, Y. Sanehira, T. Miyasaka, *J. Mater. Chem. A* **2015**, *3*, 10837–10844;

j) J. Song, E. Zheng, X.-F. Wang, W. Tian, T. Miyasaka, *Sol. Energy Mater. Sol. Cells* **2016**, *144*, 623–630.

[6] a) M. Fonrodona, J. Escarré, F. Villar, D. Soler, J. M. Asensi, J. Bertomeu, J. Andreu, *Sol. Energy Mater. Sol. Cells* **2005**, *89*, 37–47;

b) J. H. Heo, M. H. Lee, H. J. Han, B. R. Patil, J. S. Yu, S. H. Im, *J. Mater. Chem. A* **2016**, *4*, 1572–1578.

[7] Z. Zhu, Y. Bai, X. Liu, C.-C. Chueh, S. Yang, A. K. Y. Jen, *Adv. Mater.* **2016**, DOI: 10.1002/adma.201600619.

[8] a) C. Yu, J. C. Yu, F. Wang, H. Wen, Y. Tang, *CrystEngComm* **2010**, *12*, 341–343;

b) B. Bob, T.-B. Song, C.-C. Chen, Z. Xu, Y. Yang, *Chem. Mater.* **2013**, *25*, 4725–4730.

[9] a) D. E. Perea, E. R. Hemesath, E. J. Schwalbach, J. L. Lensch-Falk, P. W. Voorhees, L. J. Lauhon, *Nat. Nanotechnol.* **2009**, *4*, 315–319;

b) B. Roose, S. Pathak, U. Steiner, *Chem. Soc. Rev.* **2015**, *44*, 8326–8349;

c) Z. Q. Li, Y. L. Yin, X. D. Liu, L. Y. Li, H. Liu, Q. G. Song, *J. Appl. Phys.* **2009**, *106*, 083701;

d) V. Meller, M. Rasp, G. Štefanić, J. Ba, S. Genther, J. Rathousky, M. Niederberger, D. Fattakhova-Rohlfing, *Chem. Mater.* **2009**, *21*, 5229 – 5236.

[10] X. Feng, K. Shankar, M. Paulose, C. A. Grimes, *Angew. Chem.* **2009**, *121*, 8239–8242.

[11] E. Ramasamy, J. Lee, *Energy Environ. Sci.* **2011**, *4*, 2529–2536.

[12] Y. Shao, Y. Yuan, J. Huang, *Nat. Energy* **2016**, *1*, 15001.

[13] Z. Xiao, Q. Dong, C. Bi, Y. Shao, Y. Yuan, J. Huang, *Adv. Mater.* **2014**, *26*, 6503–6509.

[14] a) W. Chen, Y. Wu, Y. Yue, J. Liu, W. Zhang, X. Yang, H. Chen, E. Bi, I. Ashraful, M. Grätzel, L. Han, *Science* **2015**, *350*, 944–948;

b) Y. Li, Y. Zhao, Q. Chen, Y. Yang, Y. Liu, Z. Hong, Z. Liu, Y.-T. Hsieh, L. Meng, Y. Li, Y. Yang, *J. Am. Chem. Soc.* **2015**, *137*, 15540–15547.

[15] Z. Xiao, C. Bi, Y. Shao, Q. Dong, Q. Wang, Y. Yuan, C. Wang, Y. Gao, J. Huang, *Energy Environ. Sci.* **2014**, *7*, 2619–2623.

[16] Q. Wang, C. Bi, J. Huang, *Nano Energy* **2015**, *15*, 275–280.

[17] Q. Wang, Y. Shao, H. Xie, L. Lyu, X. Liu, Y. Gao, J. Huang, *Appl. Phys. Lett.* **2014**, *105*, 163508.

Supplementary figures S1 & S2 follow.

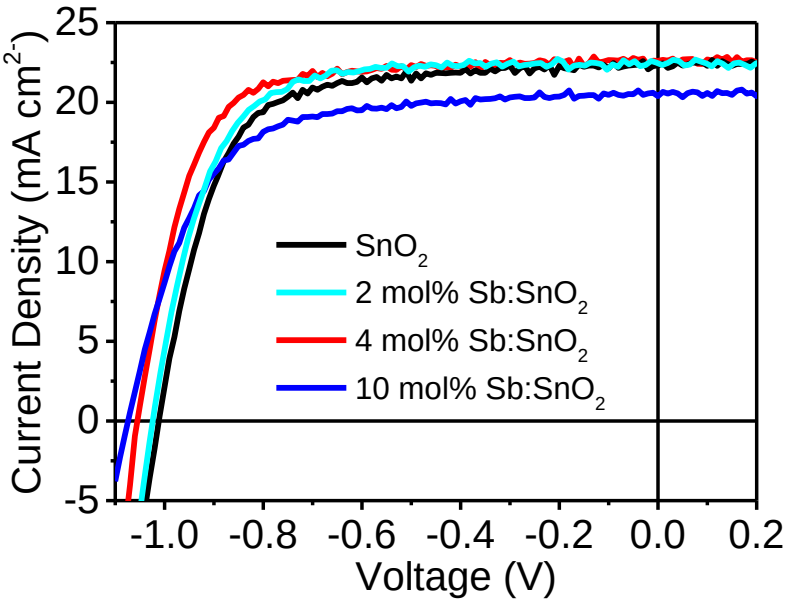

Figure S1 *J-V* curves of typical perovskite device fabricated with pristine SnO_2 and $Sb:SnO_2$ with various doping levels.

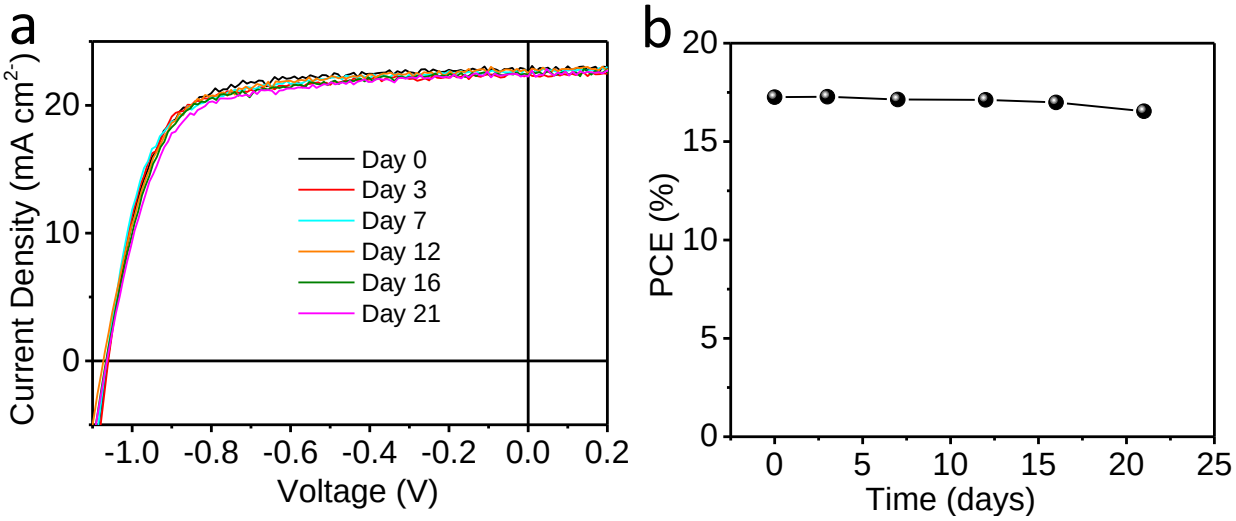

Figure S2 (a) *J-V* curves of typical perovskite device fabricated with $Sb:SnO_2$ ETL stored in a desiccator under room light for various days. (b) Degradation of device PCE as a function of storage time.